Bilayers of transition metal dichalcogenides: Different stackings and heterostructures

Humberto Terrones[a)]
Department of Physics and Center for 2-D and Layered Materials, The Pennsylvania State University, University Park, Pennsylvania 16802

Mauricio Terrones[b)]
Department of Physics and Center for 2-D and Layered Materials, The Pennsylvania State University, University Park, Pennsylvania 16802; and Department of Chemistry, Department of Materials Science and Engineering and Materials Research Institute, The Pennsylvania State University, University Park, Pennsylvania 16802

(Received 10 July 2013; accepted 9 September 2013)

Besides graphene and hexagonal boron nitride, transition metal dichalcogenides (TMDs) also exhibit a layered structure in which the layers weakly interact via van der Waals forces. Semiconducting TMDs in bulk are indirect band gap materials. However, an isolated sheet exhibits a direct gap. This particular behavior makes them very attractive in terms of optical properties. Moreover, NbS_2 and $NbSe_2$ in bulk and their monolayers are metallic. Density functional theory calculations were carried out to study different TMD bilayer systems. First, different bilayer geometries with different stackings were considered. It was found that the indirect and direct band gaps compete; however, the indirect band gap always dominates. Surprisingly, bilayer heterostructures of different TMDs have been found to possess direct band gaps. Finally, heterobilayers composed of one metallic monolayer and a semiconducting layer are predicted as novel metallic van der Waals solids that might find applications in new two-dimensional nanodevices.

I. INTRODUCTION

Studies of transition metal dichalcogenides (TMDs) and the search for monolayers or two-dimensional (2D) systems are not new; monolayers of TMDs consist of metal layers sandwiched by sulfur, selenium, or tellurium atomic layers. Wilson and Yoffe[1] published a seminal paper in which the physicochemical properties of TMDs are described in detail. Perhaps the first work on MoS_2 exfoliation by the adhesive type method resulting in few-layer MoS_2 and monolayers of MoS_2 is the work of Frindt.[2] One year earlier, the same author published a manuscript in which the optical properties of few-layered MoS_2 were reported[3]: In this manuscript, the differences between the absorption spectra of thin (few layers) and bulk MoS_2 were established. Later, Joensen et al.[4] published an article entitled "single-layer MoS_2" obtained by lithium intercalation. Here, it was found that after drying the exfoliated MoS_2, the material restacked in a random fashion. As in graphite and hexagonal boron nitride, layered systems of TMDs (including inorganic fullerenes and nanotubes) are held together by weak van der Waals forces that make them suitable for lubrication.[5–7] It is noteworthy that these inorganic fullerenes and nanotubes of TMDs are formed by introducing curvature to the inorganic sheets.[8–10]

As stated in the abstract, TMDs could exhibit semiconducting (indirect and direct band gaps) and metallic behaviors depending upon their composition, structure, and number of layers. In addition, they could possess two main crystallographic phases: trigonal prismatic and octahedral (less stable). The trigonal prismatic crystal structure of MoS_2, $MoSe_2$, WS_2, and WSe_2 corresponds to indirect band gap materials, whereas their octahedral phases are metallic.[11–15] In metallic systems such as NbS_2 and $NbSe_2$, even the same trigonal prismatic structure (the same as the semiconducting TMDs already mentioned above) reveals a metallic behavior,[1,16–18] and these metals could also exhibit charge-density wave instabilities.[19,20,16] What makes the trigonal prismatic semiconducting TMDs very special is that as the number of layers decrease, the material becomes a direct band gap semiconductor when reaching a monolayer,[21] thus making it suitable for optical applications[22–30] (see Fig. 1).

Regarding early calculations of single layers of TMDs, Bromley et al.[31] used a semi empirical tight binding method for generating the band structures of MoS_2, $MoSe_2$, WS_2, WSe_2, and α-$MoTe_2$; however, the direct band gap features for the monolayers were not observed using this approach. Later, calculations using density functional theory (DFT) and GW approaches confirmed the direct band gap

[a)]Address all correspondence to this author.
e-mail: hzt2@psu.edu
[b)]This author was an editor of this focus issue during the review and decision stage. For the *JMR* policy on review and publication of manuscripts authored by editors, please refer to http://www.mrs.org_jmr_policy.
DOI: 10.1557/jmr.2013.284

 © Materials Research Society 2013

https://doi.org/10.1557/jmr.2013.284 Published online by Cambridge University Press

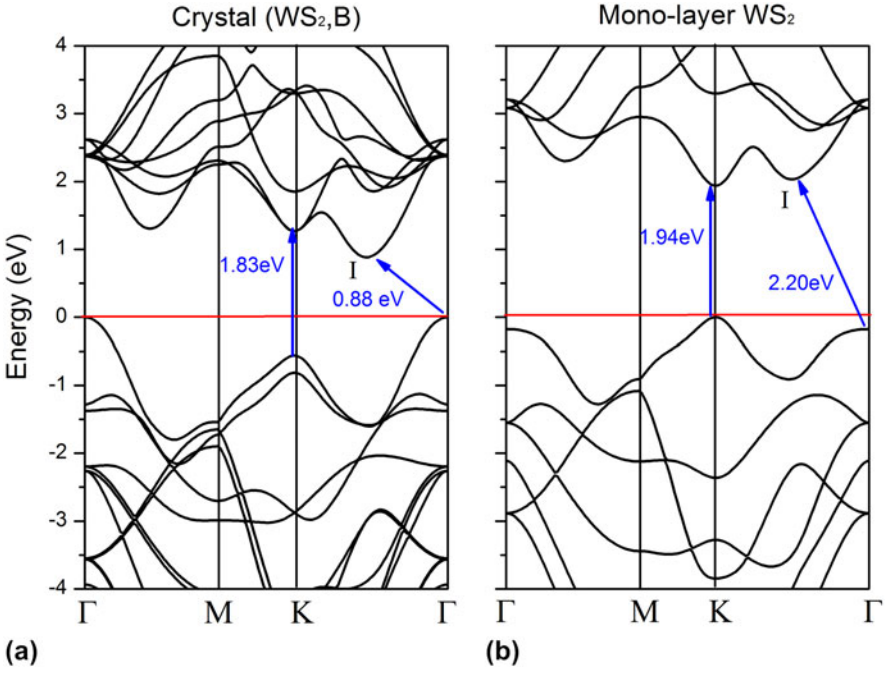


FIG. 1. Band structures for WS_2 showing the direct band gap K–K and the indirect band gap Γ–I for (a) WS_2 crystal (b) WS_2 monolayer. The line at 0 eV shows the top of the valence band.

existence at the K point[32–37] (see Fig. 1). It looks like this direct band gap behavior is restricted only to monolayers of TMDs, but to the best of our knowledge, there are no studies so far demonstrating that bilayers might reveal a direct band gap. Therefore, a detailed study on the electronic behavior of bilayers becomes necessary including different stackings of monolayers with the same TMD composition, and heterolayers with different types of layered materials, and this is precisely the aim of this work.

Our calculations indicate that bilayer WS_2 with different stackings reveals different band structures in which the energy differences between the direct and indirect gaps are small. Nevertheless, the indirect band gap continues to be dominant. This behavior can also be extended to the other semiconducting TMDs such as MoS_2, $MoSe_2$, and WSe_2 (see below). To our surprise, when studying heterobilayer systems of TMDs (WS_2–WSe_2, MoS_2–$MoSe_2$, WSe_2–MoS_2, and $MoSe_2$–WS_2), direct band gaps, half in energy of those reported for monolayers, are found for some cases in which the diselenide layer is sandwiched with a disulfide layer.[37] These direct band gaps range from 0.79 to 1.16 eV. Therefore, the study of heterobilayers of TMDs becomes relevant for designing and constructing novel optoelectronic materials. At the same time, metallic and semiconducting bilayer heterostructures have been also calculated finding that all the systems studied possess a metallic behavior, but with unique features above the Fermi level for the MoS_2–$NbSe_2$ and WS_2–$NbSe_2$ systems that are discussed in the following sections.

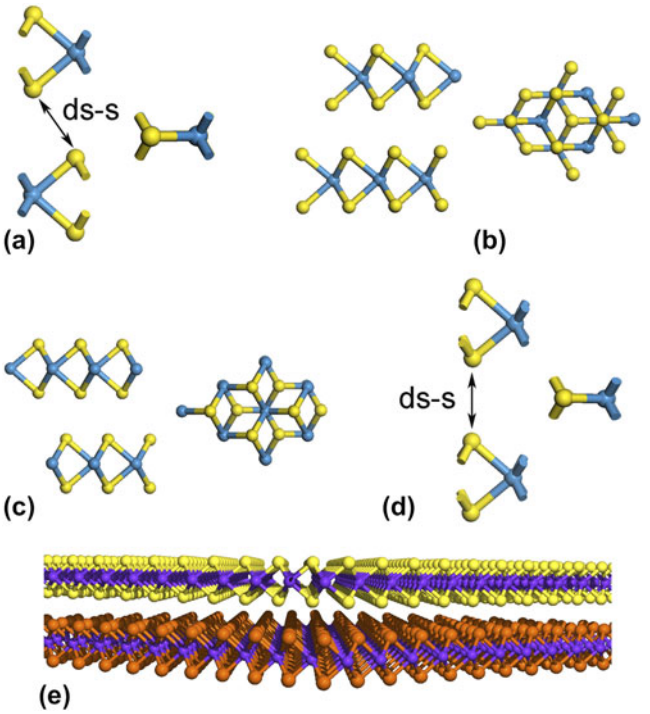


FIG. 2. Different stackings for bilayer WS_2 systems obtained by displacing one layer with respect to the other. (a) Side and top view of bulk like stacking or bilayer(WS_2, B); the arrow shows the distance between chalcogen "d_{s-s}" atoms between the layers. (b) Side and top view of AB1-type stacking or bilayer(WS_2, AB1). (c) Side and top view of AB2-type stacking or bilayer(WS_2, AB2). (d) Side and top view of A-type stacking or bilayer(WS_2, A); the arrow shows the distance between chalcogen "d_{s-s}" atoms between the layers. (e) Heterobilayer of MoS_2 and $MoSe_2$.

https://doi.org/10.1557/jmr.2013.284 Published online by Cambridge University Press

A. Band gap competition in different stackings of TMDs

To shed light on the behavior of bilayers of TMDs with different stackings, four cases of WS_2 bilayers have been studied: (i) crystal-type stacking called bilayer (WS_2, B), where B stands for bulk. This is the stacking presented in the WS_2 triangular prismatic phases of TMDs, where the metal atoms are on top of the sulfur atoms [see Fig. 2(a)]; (ii) bilayer (WS_2, AB1) stacking in which the layers are displaced such that the transition metal atoms of one layer are in the center of the hexagonal WS_2 rings of the other TMD layer as shown in Fig. 2(b); (iii) bilayer (WS_2, AB2) where the displacement produces the metal atoms of one layer to be on top of metal atoms of the other, and the sulfurs on one layer in the center of the hexagonal WS_2 rings of the other layer [see Fig. 2(c)], and (iv) bilayer (WS_2, A) in which the metal atoms are on top of metal atoms and chalcogen atoms on top of chalcogen atoms [see Fig. 2(d)]. When calculating these systems using DFT-local density approximation (LDA) (see Sec. IV),

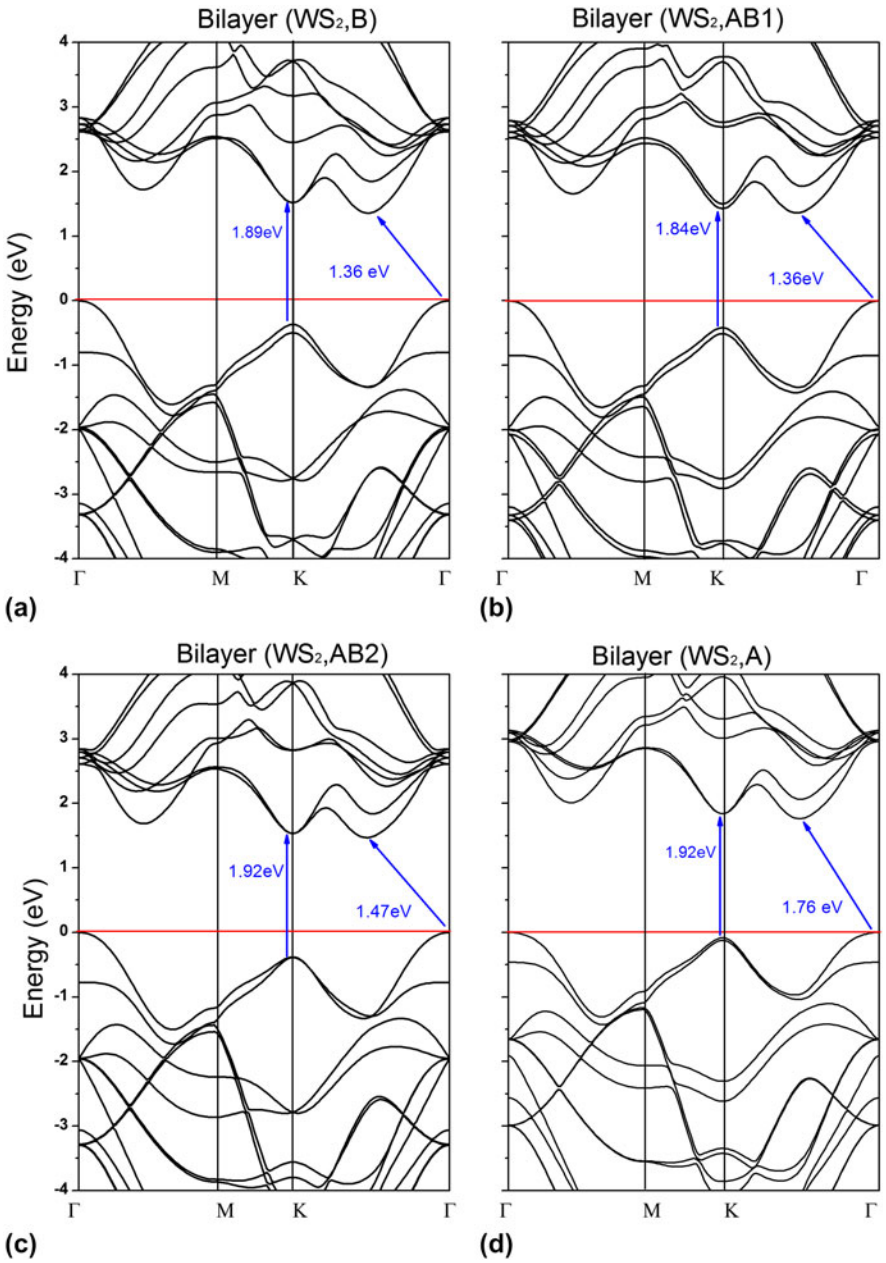


FIG. 3. Band structure for different WS_2 bilayer stackings showing the directs K–K band gap and the indirect band gap Γ–I. (a) bilayer(WS_2, B), (b) bilayer(WS_2, AB1), (c) bilayer(WS_2, AB2), (d) bilayer(WS_2, A). The line at 0 eV shows the top of the valence band.

https://doi.org/10.1557/jmr.2013.284 Published online by Cambridge University Press

TABLE I. Semiconducting TMDs' properties as calculated with DFT-LDA showing the indirect band gap, the direct band gap, the difference between direct and indirect gaps, lattice parameters, distance between chalcogen atoms (d_{s-s} or d_{se-se}) between the two layers in parenthesis, and relative energies per cell. In the case of the crystals for which the experimental lattice parameters are known, these are put in parenthesis with the prefix "exp."

Structure	Indirect gap (eV)	Direct gap (eV)	ΔGap (eV)	Lattice "a" (Å) and (distance between chalcogen atoms in Å).	Relative energy/cell (eV)
Bilayer (WS_2, A)	1.762 (Γ–I)	1.922 (K–K)	0.160	3.145 (d_{s-s} = 3.677)	0.1797
Bilayer (WS_2, B)	1.357 (Γ–I)	1.890 (K–K)	0.533	3.146 (d_{s-s} = 3.458)	0.1089
Crystal (WS_2, A)	1.417 (Γ–I)	1.903 (K–K)	0.486	3.146 (d_{s-s} = 3.680)	0.0699
Crystal (WS_2, B)	0.883 (Γ–I)	1.829 (K–K)	0.946	a = 3.147 (3.155 exp[38]) c = 12.166 (12.35 exp[38])	0
Single-layer WS_2	2.209 (Γ–I)	1.940 (K–K)	−0.268	3.146	0.2198
Bilayer (MoS_2, A)	1.589 (Γ–I)	1.801 (K–K)	0.213	3.167 (d_{s-s} = 3.646)	0.1975
Bilayer (MoS_2, B)	1.112 (Γ–I)	1.773 (K–K)	0.662	3.168 (d_{s-s} = 3.412)	0.0775
Crystal (MoS_2, A)	1.268 (Γ–I)	1.778 (K–K)	0.510	3.168 (d_{s-s} = 3.643)	0.1556
Crystal (MoS_2, B)	0.706 (Γ-I)	1.714 (K–K)	1.008	a = 3.170 (3.160 exp[38]) c = 12.106 (12.29 exp[38])	0
Single-layer MoS_2	2.031 (Γ–I)	1.823 (K–K)	−0.207	3.167	0.2398
Bilayer (WSe_2, A)	1.515 (K–I) 1.707 (Γ–I)	1.658 (K–K)	0.143–0.049	3.268 (d_{se-se} = 3.842)	0.2017
Bilayer (WSe_2, B)	1.292	1.618 (K–K)	0.326	3.269 (d_{se-se} = 3.619)	0.1217
Crystal (WSe_2, A)	1.354 (K–I) 1.409 (Γ–I)	1.728 (K–K)	0.282 0.226	3.269 (d_{se-se} = 3.876)	0.0786
Crystal (WSe_2, B)	0.890 (Γ–I)	1.551 (K–K)	0.661	a = 3.271 (3.288 exp[39]) c = 12.875 (13.00 exp[39])	0
WSe_2-single-layer	2.145 (Γ–I)	1.676 (K–K)	−0.469	3.268	0.2466
Bilayer ($MoSe_2$, A)	1.432 (K–I) 1.548 (Γ–I)	1.579 (K–K)	0.147 0.031	3.286 (d_{se-se} = 3.850)	0.2163
Bilayer ($MoSe_2$, B)	1.047 (Γ–I)	1.550 (K–K)	0.5039	3.287 (d_{se-se} = 3.586)	0.1302
Crystal ($MoSe_2$, A)	1.279 (K–I) 1.257 (Γ-I)	1.629 (K–K)	0.272 0.294	3.287 (d_{se-se} = 3.845)	0.0849
Crystal ($MoSe_2$, B)	0.686 (Γ–I)	1.483 (K–K)	0.797	a = 3.290 (3.288 exp[40]) c = 12.779 (12.931 exp[40])	0
$MoSe_2$-single-layer	1.973	1.606 (K–K)	−0.367	3.285	0.2628

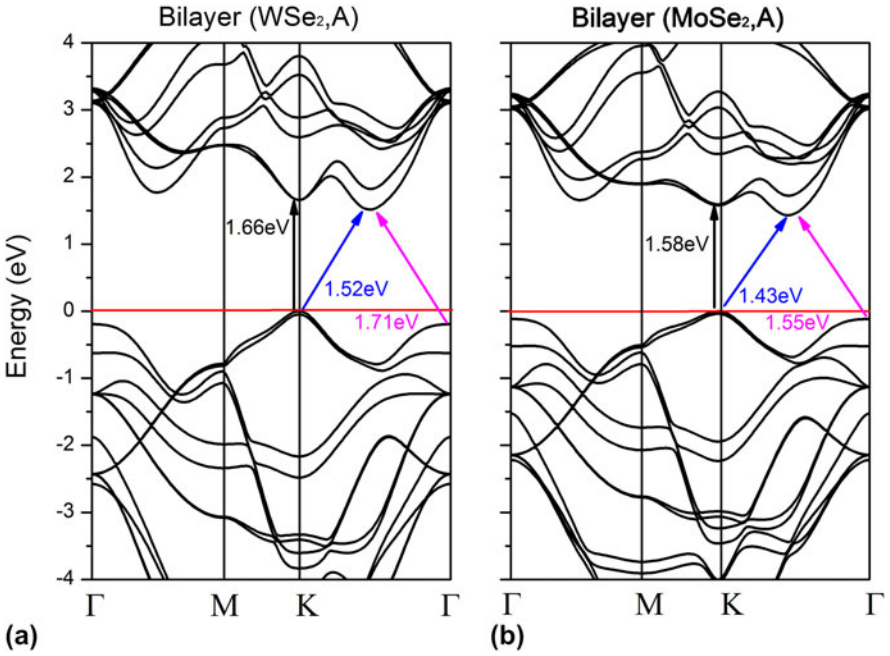


FIG. 4. (a) Band structure for the bilayer(WSe_2, A) showing the direct K–K band gap (black) and the indirect Γ–I (magenta) and K–I (blue) band gaps. Note that the direct band gap is smaller than the indirect Γ–I for this case. (b) Band structure for the bilayer($MoSe_2$, A) showing the direct K–K band gap and the indirect Γ–I and K–I band gaps. Note here that the direct band gap and the indirect band gap Γ–I are very close. However in both cases (a) and (b), the indirect band gaps K–I are smaller than the direct band gap; this might be observed experimentally by photoluminescence or optical absorption techniques. The line at 0 eV shows the top of the valence band.

https://doi.org/10.1557/jmr.2013.284 Published online by Cambridge University Press

it was found that the smallest gap difference between direct (K–K) and indirect (Γ–I) band gaps for the bilayer (WS_2, A) was 0.16 eV (see Fig. 3). However, in all cases the indirect band gap dominates with gap differences ranging from 0.53 eV in bilayer (WS_2, B) to 0.16 in bilayer (WS_2, A). In addition, both the direct and indirect band gaps change when modifying the stacking, and it was also noted that the indirect band gap exhibits a more significant change from 1.36 to 1.76 eV (see Fig. 3). Since the smallest difference of direct and indirect band

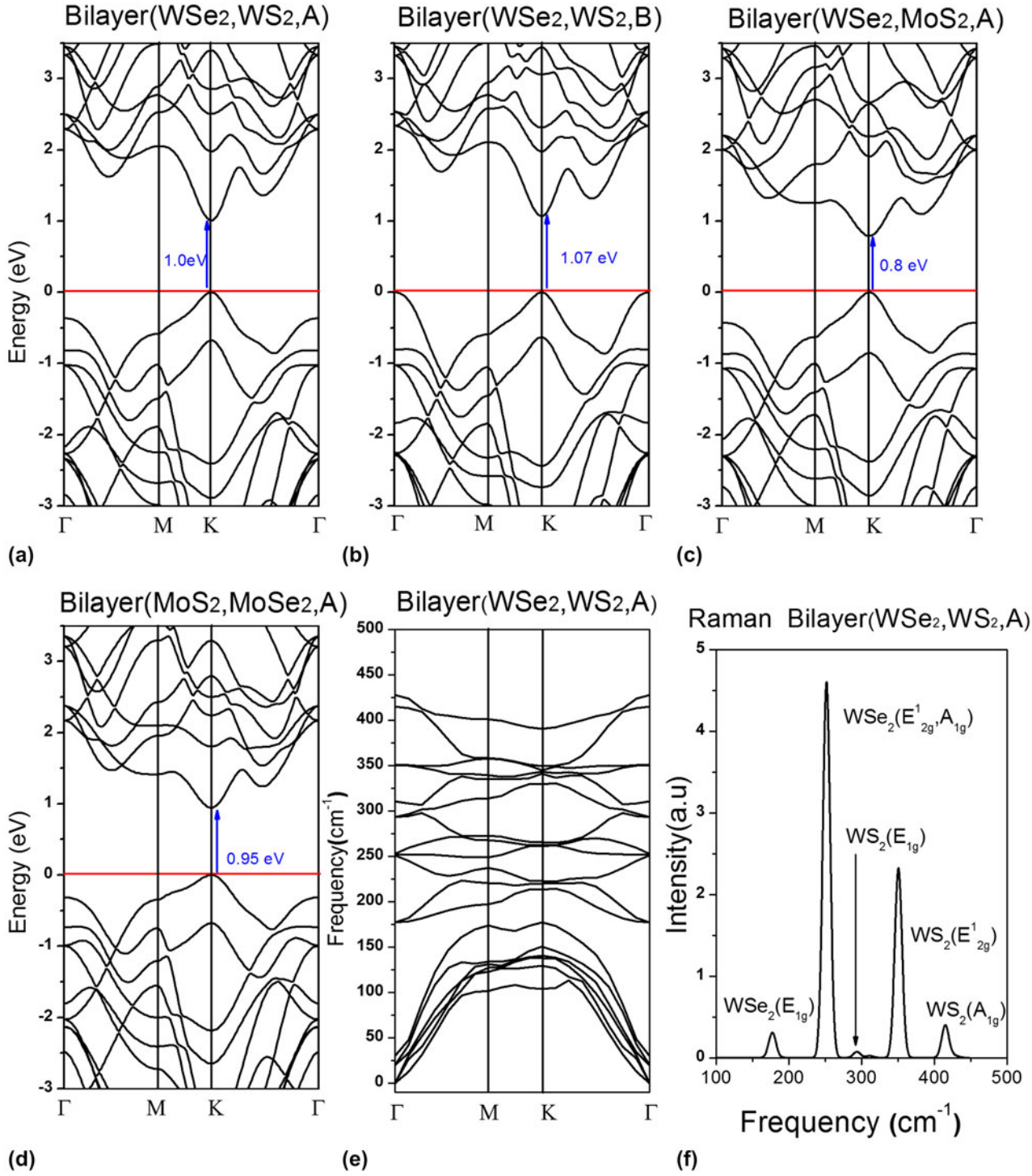


FIG. 5. Direct band gaps at K point in hetero bilayer semiconducting TMD. (a) Bilayer(WSe_2, WS_2, A), (b) bilayer(WSe_2, WS_2, B), (c) bilayer(WSe_2, MoS_2, A), (d) bilayer(MoS_2–$MoSe_2$, A). (e) Phonon dispersion of bilayer(WSe_2, WS_2, A). (f) Calculated Raman intensities of bilayer(WSe_2, WS_2, A).

https://doi.org/10.1557/jmr.2013.284 Published online by Cambridge University Press

gaps is achieved with stacking type A, we have calculated the direct and indirect band gaps for other semiconducting TMD bilayers considering stacking A for MoS_2, WSe_2, and $MoSe_2$ (see Table I). Interestingly, it was found that bilayer (WSe_2, A) reveals a smaller direct band gap at K–K when compared to the indirect band gap Γ–I, with a difference of 0.049 eV, nevertheless, the material continues being an indirect band gap semiconductor since the indirect band gap K–I is smaller than the direct band gap at K [see Fig. 4(a)]. A similar behavior is presented by the bilayer ($MoSe_2$, A), where the difference between direct band gap K–K and indirect band gap Γ–I is very small with a value of 0.031 eV [see Fig. 4(b)]. Therefore, the diselenide bilayers show a different electronic behavior from the disulfides [see Fig. 2(e)]. In general, for bilayers and the crystals of MoS_2, $MoSe_2$, WS_2, and WSe_2, the stacking type A possesses a smaller band gap than the stacking type B found in the trigonal prismatic phases. However, stacking type B are more favorable in energy (see Table I).

B. Semiconducting heterobilayers of TMDs

Motivated by the results discussed above, 24 heterobilayers of TMDs (MoS_2, $MoSe_2$, WS_2, and WSe_2) have been calculated using the DFT-LDA approach considering crystalline phases with different stackings. To name these systems, the following nomenclature was used: bilayer (MoS_2, WSe_2, A), where it is established if the system is a bilayer or a crystal, in parenthesis, the first two indices correspond to each of the TMDs involved, and the third index reveals the type of stacking as shown in Sec. I. A (B for bulk and A as shown in Fig. 2). These systems can be categorized into four groups depending on their band structure as shown in Table II.[37] Interestingly, some cases exhibit direct band gaps at the K point, which are approximately half of those found in the pure single layers (see Table II and Fig. 5). Details of these systems have been published recently.[37] Therefore, direct band gap semiconductors out of heterobilayers are possible if diselenides are mixed with disulfides. It is worth mentioning that to achieve this, the disulfide layer needs to be expanded and the diselenide exhibits a small reduction. The distance between chalcogen atoms between layers (see Fig. 2) is larger for the stacking type A than for the stacking type B (see Table III); therefore, the interlayer distance is slightly bigger in the stacking type A. Despite the strain, phonon dispersion calculations indicate that these systems are structurally stable showing no imaginary frequencies [see Fig. 5(e)]. In addition, the phonon dispersion provides the vibrational modes observed in Raman spectroscopy which are closer to the experimental values[37] [see Figs. 5(e) and 5(f)].

II. METALLIC HETEROBILAYERS OF TMDs

NbS_2 and $NbSe_2$ in bulk and their monolayers possess metallic behavior [see Figs. 6(a) and 6(b)]. Therefore, it is relevant to study heterobilayers of TMDs in which one layer is semiconducting and the other metallic. The studied cases include MoS_2–NbS_2, MoS_2–$NbSe_2$, WS_2–NbS_2, WS_2–$NbSe_2$, $MoSe_2$–NbS_2, $MoSe_2$–$NbSe_2$, WSe_2–NbS_2, and WSe_2–$NbSe_2$. It was found that all cases are metallic, however, the MoS_2–$NbSe_2$ and WS_2–$NbSe_2$ bilayer systems exhibit a particular band structure above the

TABLE II. Direct and indirect (in parenthesis) band gaps in eV of hybrids of semiconducting TMDs. Systems with a dominant direct band gap at the K point in the Brillouin zone have an asterisk "*". Cases with "+" show an indirect fundamental band gap Γ–K, and "&" corresponds to a dominant indirect gap K–I.

Hybrid structure	Bilayer stacking A	Bilayer stacking B	Crystal stacking A	Crystal stacking B
WS_2–MoS_2 type 1	1.695 (1.586 Γ–I)	1.708 (1.190 Γ–I)	1.669 (1.284 Γ–I)	1.664 (0.764 Γ–I)
WS_2–WSe_2 type 2	1.007 (1.725 Γ–I)*	1.068 (1.314 Γ–I)*	1.007 (1.406 Γ–I)*	1.037 (0.883 Γ–I)
MoS_2–WSe_2 type 2	0.790 (1.525 Γ–I)*	0.891 (1.147 Γ–I)*	0.802 (1.245 Γ–I)*	0.883 (0.736 Γ–I)
WS_2–$MoSe_2$ type 3	1.154 (1.594 Γ–I)*	1.180 (1.052 Γ–K)$^{+}$	1.157 (1.316 Γ–I)*	1.155 (0.790 Γ–I)
MoS_2–$MoSe_2$ type 3	0.945 (1.560 Γ–I)*	1.013 (0.899 Γ–K)$^{+}$	0.949 (1.260 Γ–I)*	0.998 (0.699 Γ–I)
WSe_2–$MoSe_2$ type 4	1.443 (1.330 K–I)$^{\&}$	1.471 (1.116 Γ–I)	1.444 (1.215 K–I)$^{\&}$	1.418 (0.761 Γ–I)

TABLE III. Lattice parameters "*a*" in Å, and distance d_{s-se} (in parenthesis, in Å) between chalcogen atoms between the two layers of the TMDs.

Hybrid structure	Bilayer stacking A	Bilayer stacking B	Crystal stacking A	Crystal stacking B
WS_2–MoS_2	3.155 (3.686)	3.157 (3.439)	3.156 (3.671)	3.158 (3.441)
WS_2–WSe_2	3.204 (3.763)	3.205 (3.527)	3.204 (3.763)	3.206 (3.531)
MoS_2–WSe_2	3.218 (3.765)	3.219 (3.522)	3.218 (3.734)	3.220 (3.502)
WS_2–$MoSe_2$	3.210 (3.768)	3.211 (3.521)	3.211 (3.769)	3.213 (3.523)
MoS_2–$MoSe_2$	3.225 (3.768)	3.226 (3.497)	3.226 (3.740)	3.228 (3.499)
WSe_2–$MoSe_2$	3.277 (3.833)	3.278 (3.584)	3.277 (3.844)	3.280 (3.601)
WS_2–$NbSe_2$	3.262 (3.622)	3.264 (3.482)	...	...
MoS_2–$NbSe_2$	3.286 (3.552)	3.283 (3.445)	...	...

https://doi.org/10.1557/jmr.2013.284 Published online by Cambridge University Press

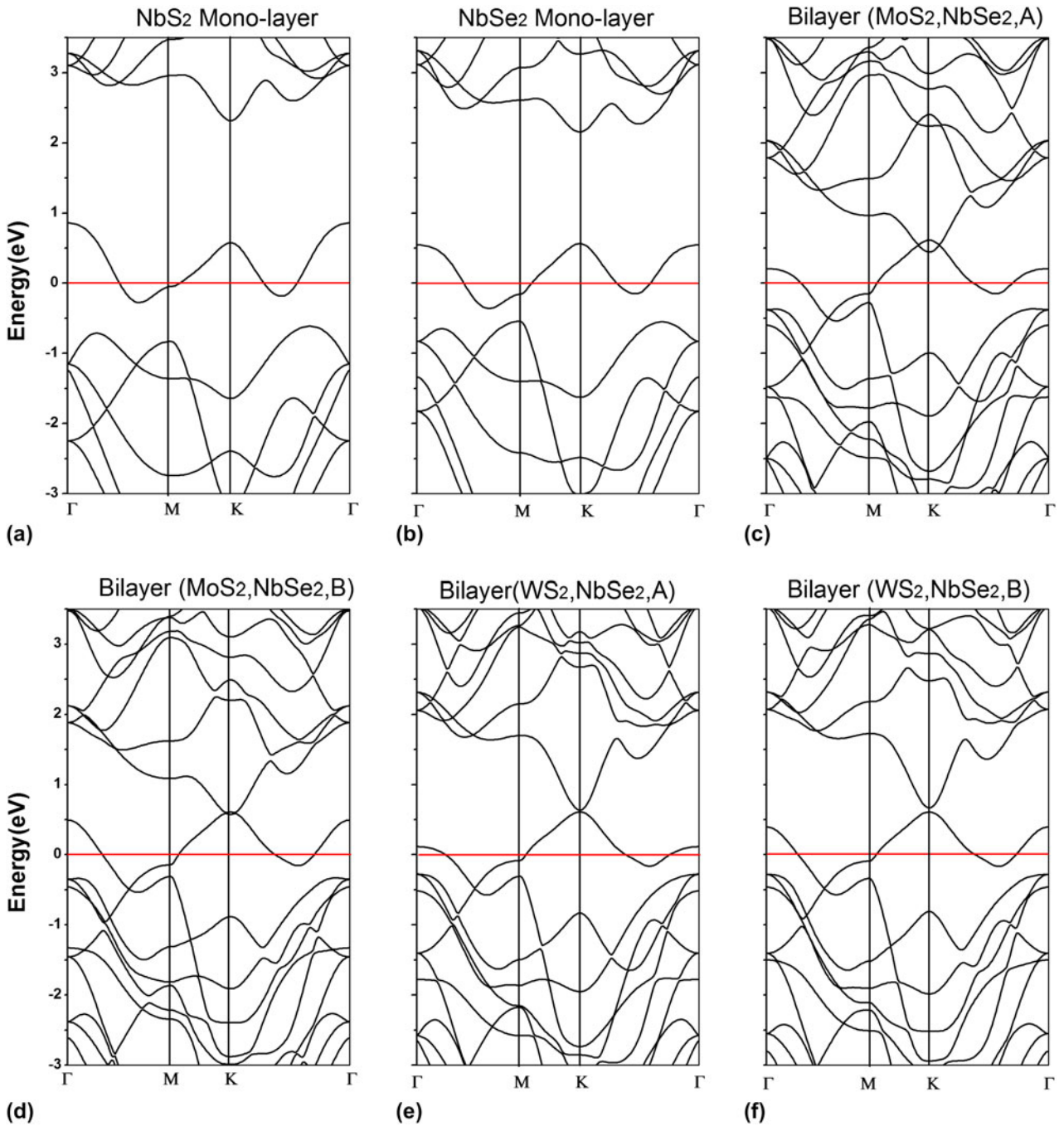


FIG. 6. Band structure of metallic TMD. (a) NbS_2 monolayer, (b) $NbSe_2$ monolayer, (c) bilayer(MoS_2–$NbSe_2$, A), (d) bilayer(MoS_2–$NbSe_2$, B), (e) bilayer(WS_2–$NbSe_2$, A), and (f) bilayer(WS_2–$NbSe_2$, B). The Fermi level is at zero.

Fermi level for both stackings studied (A and B). Bilayer (MoS_2–$NbSe_2$, B) exhibited an interpenetration in the band structure, which increases for stacking A [see Figs. 6(c) and 6(d)]. For bilayer (WS_2–$NbSe_2$, B), there is a small band gap of 0.055 eV around 0.6 eV. This gap is reduced when the stacking becomes type A to 0.025 eV [see Figs. 6(e) and 6(f)]. As in the semiconducting heterobilayers, the interlayer spacing is slightly greater for stacking type A (see Table III). The partial density of states has also been computed to show that the electronic states at the Fermi level are due to the NbS_2 layer, and the disulfide layer states play a role above the Fermi level around 0.6 eV, where a crossing or almost touching of bands occur (see Fig. 7); this suggest that doping or defects might shift the Fermi level to the band touching area, thus generating a new type of "semimetal" unique in TMDs.

https://doi.org/10.1557/jmr.2013.284 Published online by Cambridge University Press

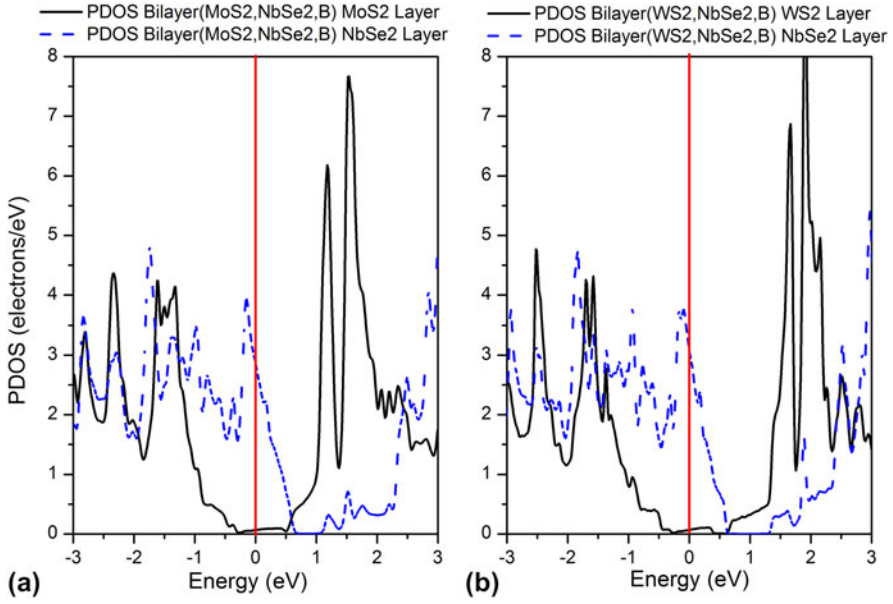


FIG. 7. PDOS of (a) bilayer(MoS_2, $NbSe_2$, B) and (b) bilayer(WS_2, $NbSe_2$, B). In both cases, the electronic states at the Fermi level are mainly due to the $NbSe_2$ layer (Fermi level is at zero).

III. CONCLUSION

It has been shown first that different stackings of TMDs play a role in their electronic properties by changing the direct band gap at the K point and also the indirect band gap Γ–I. Second, in the search for direct band gap materials with different stacking arrays exhibiting two layers of the same TMDs, it was found that although the direct and indirect band gaps become closer for a particular stacking (type A), the indirect band gap continues to dominate. However, when layers of disulfides and diselenides are sandwiched forming heterobilayer systems, a direct band gap is possible. This direct gap is half of that found in single layer TMDs, thus belonging to the infrared part of the spectrum, not to the visible as the monolayers of semiconducting TMDs. The application of these heterobilayer systems, which do not possess inversion symmetry, might find a place in new valleytronic devices. Third, heterobilayers of TMDs involving one metallic and one semiconducting layer have been analyzed finding that these exhibit metallic behavior with particular band features above the Fermi level, which might be exploited by doping or defects generating possibly new semi metallic bilayers of TMDs. Among the techniques used to synthesize these materials, chemical vapor deposition looks promising for obtaining different stackings and even different TMD layers.[41] Nevertheless, exfoliation techniques followed by annealing and pressure control might also prove useful for designing heterobilayer systems out of TMDs. Devices with heterolayers involving graphene (semimetal) and semiconducting TMDs such as WS_2 have already proved to be useful as vertical field-effect transistors;[42] therefore, the next step is to include different TMD heterostructures (semiconducting and metallic) with lattice that would match much better among them than with graphene or BN. The cases studied in this account open up the spectrum of possible applications for 2D materials (also termed van der Waals solids), thus adding new properties to the already known properties of graphene, hexagonal boron nitride, and single layer TMDs.

IV. METHODS

Our calculations have been performed using the plane wave code CASTEP,[43] on hexagonal cells under the LDA considering the Ceperley–Alder–Perdew and Zunger (CA–PZ)[44,45] functional with $9 \times 9 \times 3$ Monkhorst–Pack K-points and a plane waves cut off of 500 eV. All the structures were relaxed, including the cells, until the forces became smaller than 0.01 eV/Å and the energy tolerances were less than 5×10^{-6} eV/atom. A vacuum of 16 Å between the bilayers was considered. To select the optimum approach for interlayer distances, van der Waals interactions were considered through a dispersion correction (DFT-D)[46] under both the LDA and general gradient approximation (GGA-PW91).[47] To test the results, several TMD structures were calculated such as WS_2, MoS_2, WSe_2, $MoSe_2$, $NbSe_2$, and NbS_2 and compared with the experimental data available. The lattice constant experimental values exhibit good agreement with the LDA approach (without considering the dispersion correction DFT-D). For the LDA-DFT-D, the layers get closer to each other producing a compactification of the "*c*" lattice parameter (around 3.6% smaller than bulk), whereas with the

https://doi.org/10.1557/jmr.2013.284 Published online by Cambridge University Press

GGA-DFT-D approach, the layers get farther apart thus producing a lattice with a much larger "*c*" parameter (around 3.5% bigger than bulk). The lattice "*c*" parameters obtained with LDA produce the best fit within 1.5% or less of those reported experimentally. Moreover, our results are in agreement with those reported by other groups within the LDA formalism.[48,49] Although GGA might usually provide corrections that best describe the system, for few-layer systems with van der Waals interactions such as TMDs, LDA provides better values (compared with the experimental) for direct optical band gaps and lattice parameters. Both the DFT and GGA underestimate the electronic band gap; however, due to a coincidence, the LDA direct band gaps agree better with the experimental optical transitions observed in the photoluminescence characterization of monolayer TMDs. Therefore, we decided to use LDA for all the calculations presented here. The phonon dispersion is calculated with the above parameters but extending the plane wave cut off to 720 eV using the density functional perturbation theory as implemented in the CASTEP code, which uses the linear response methodology that works well for insulators.[50]

ACKNOWLEDGMENTS

This work is supported by the U.S. Army Research Office MURI Grant No. W911NF-11-1-0362, supported in part by the Materials Research Computing and Cyberinfrastructure unit of Information Technology Services and Penn-State Center for Nanoscale Science. M.T. also acknowledges support from the Penn State Center for Nanoscale Science for seed grant on 2-D layered materials (Grant No. DMR-0820404).

REFERENCES

1. J.A. Wilson and A.D. Yoffe: Transition metal dichalcogenides discussion and interpretation of observed optical, electrical and structural properties. *Adv. Phys.* **18**(73), 193 (1969).
2. R.F. Frindt: Single crystals of MoS_2 several molecular layers thick. *J. Appl. Phys.* **37**(4), 1928 (1966).
3. R.F. Frindt: Optical absorption of a few unit-cell layers of MoS_2. *Phys. Rev.* **140**(2A), 536 (1965).
4. P. Joensen, R.F. Frindt, and S.R. Morrison: Single-layer MoS_2. *Mater. Res. Bull.* **21**(4), 457 (1986).
5. P.D. Fleischauer: Fundamental-aspects of the electronic-structure, materials properties and lubrication performance of sputtered MoS_2 Films. *Thin Solid Films* **154**(1–2), 309 (1987).
6. J.M. Martin, C. Donnet, T. Lemogne, and T. Epicier: Superlubricity of molybdenum-disulfide. *Phys. Rev. B* **48**(14), 10583 (1993).
7. L. Rapoport, N. Fleischer, and R. Tenne: Applications of WS_2 (MoS_2) inorganic nanotubes and fullerene-like nanoparticles for solid lubrication and for structural nanocomposites. *J. Mater. Chem.* **15**(18), 1782 (2005).
8. R. Tenne, L. Margulis, M. Genut, and G. Hodes: Polyhedral and cylindrical structures of tungsten disulfide. *Nature* **360**(6403), 444 (1992).
9. L. Margulis, G. Salitra, R. Tenne, and M. Talianker: Nested fullerene-like structures. *Nature* **365**(6442), 113 (1993).
10. R. Tenne, L. Margulis, and G. Hodes: Fullerene-like nanocrystals of tungsten disulfide. *Adv. Mater.* **5**(5), 386 (1993).
11. L. Mattheis: Band structures of transition-metal-dichalcogenide layer compounds. *Phys. Rev. B* **8**(8), 3719 (1973).
12. F. Wypych and R. Schollhorn: 1T-MOS_2, a new metallic modification of molybdenum-disulfide. *J. Chem. Soc. Chem. Commun.* (19), 1386 (1992).
13. D. Yang, S.J. Sandoval, W.M.R. Divigalpitiya, J.C. Irwin, and R.F. Frindt: Structure of single-molecular-layer MOS_2. *Phys. Rev. B* **43**(14), 12053 (1991).
14. R. Bissessur, M.G. Kanatzidis, J.L. Schindler, and C.R. Kannewurf: Encapsulation of polymers into MOS_2 and metal to insulator transition in metastable MOS_2. *J. Chem. Soc. Chem. Commun.* (20), 1582 (1993).
15. V. Petkov, S.J.L. Billinge, J. Heising, and M.G. Kanatzidis: Application of atomic pair distribution function analysis to materials with intrinsic disorder. Three-dimensional structure of exfoliated-restacked WS_2: Not just a random turbostratic assembly of layers. *J. Am. Chem. Soc.* **122**(47), 11571 (2000).
16. D.J. Rahn, S. Hellmann, M. Kallane, C. Sohrt, T.K. Kim, L. Kipp, and K. Rossnagel: Gaps and kinks in the electronic structure of the superconductor 2H-$NbSe_2$ from angle-resolved photoemission at 1 K. *Phys. Rev. B* **85**(22), 224532 (2012).
17. T.K. Wieting and M. Schluter: *Electrons and Phonons in Layered Crystal Structures* (D. Reidel, Dordrecht, Netherlands, 1979).
18. G. Seifert, H. Terrones, M. Terrones, and T. Frauenheim: Novel NbS_2 metallic nanotubes. *Solid State Commun.* **115**(12), 635 (2000).
19. D.E. Moncton, J.D. Axe, and F.J. Disalvo: Neutron-scattering study of charge-density wave transitions in 2H-$TaSe_2$ and 2H-$NbSe_2$. *Phys. Rev. B* **16**(2), 801 (1977).
20. C.D. Malliakas and M.G. Kanatzidis: Nb-Nb interactions define the charge density wave structure of 2H-$NbSe_2$. *J. Am. Chem. Soc.* **135**(5), 1719 (2013).
21. K.F. Mak, C. Lee, J. Hone, J. Shan, and T.F. Heinz: Atomically thin MoS_2: A new direct-gap semiconductor. *Phys. Rev. Lett.* **105**(13), 136805 (2010).
22. H.L. Zeng, J.F. Dai, W. Yao, D. Xiao, and X.D. Cui: Valley polarization in MoS_2 monolayers by optical pumping. *Nat. Nanotechnol.* **7**(8), 490 (2012).
23. K.F. Mak, K.L. He, J. Shan, and T.F. Heinz: Control of valley polarization in monolayer MoS_2 by optical helicity. *Nat. Nanotechnol.* **7**(8), 494 (2012).
24. H. Wang, L.L. Yu, Y.H. Lee, Y.M. Shi, A. Hsu, M.L. Chin, L.J. Li, M. Dubey, J. Kong, and T. Palacios: Integrated circuits based on bilayer MoS_2 transistors. *Nano Lett.* **12**(9), 4674 (2012).
25. W.S. Hwang, M. Remskar, R.S. Yan, V. Protasenko, K. Tahy, S.D. Chae, P. Zhao, A. Konar, H.L. Xing, A. Seabaugh, and D. Jena: Transistors with chemically synthesized layered semiconductor WS_2 exhibiting 105 room temperature modulation and ambipolar behavior. *Appl. Phys. Lett.* **101**(1), 013107 (2012).
26. Y.J. Zhang, J.T. Ye, Y. Matsuhashi, and Y. Iwasa: Ambipolar MoS_2 thin flake transistors. *Nano Lett.* **12**(3), 1136 (2012).
27. H. Fang, S. Chuang, T.C. Chang, K. Takei, T. Takahashi, and A. Javey: High-performance single layered WSe_2 p-FETs with chemically doped contacts. *Nano Lett.* **12**(7), 3788 (2012).
28. Q.A. Wang, K. Kalantar-Zadeh, A. Kis, J.N. Coleman, and M.S. Strano: Electronics and optoelectronics of two-dimensional transition metal dichalcogenides. *Nat. Nanotechnol.* **7**, 699 (2012).
29. N. Perea-López, A.L. Elías, A. Berkdemir, A. Castro-Beltran, H.R. Gutiérrez, S. Feng, R. Lv, T. Hayashi, F. López-Urías, S. Ghosh, B. Muchharla, S. Talapatra, H. Terrones, and M. Terrones: Photosensor device based on few-layered WS_2 Films. *Adv. Funct. Mater.* (2013) DOI: 10.1002/adfm.201300760.
30. M. Chhowalla, H.S. Shin, G. Eda, L.J. Li, K.P. Loh, and H. Zhang: The chemistry of two-dimensional layered transition metal dichalcogenide nanosheets. *Nat. Chem.* **5**(4), 263 (2013).

https://doi.org/10.1557/jmr.2013.284 Published online by Cambridge University Press

31. R.A. Bromley, A.D. Yoffe, and R.B. Murray: Band structures of some transition-metal dichalcogenides. III. Group VIA-trigonal prism materials. *J. Phys. C: Solid State Phys.* **5**(7), 759 (1972).
32. S. Lebegue and O. Eriksson: Electronic structure of two-dimensional crystals from ab initio theory. *Phys. Rev. B* **79**(11), 115409 (2009).
33. T. Boker, R. Severin, A. Muller, C. Janowitz, R. Manzke, D. Voss, P. Kruger, A. Mazur, and J. Pollmann: Band structure of MoS_2, $MoSe_2$, and alpha-$MoTe_2$: Angle-resolved photoelectron spectroscopy and ab initio calculations. *Phys. Rev. B* **64**(23), 235305 (2001).
34. H. Jiang: Electronic band structures of molybdenum and tungsten dichalcogenides by the GW approach. *J. Phys. Chem. C* **116**(14), 7664 (2012).
35. T. Cheiwchanchamnangij and W.R.L. Lambrecht: Quasiparticle band structure calculation of monolayer, bilayer, and bulk MoS_2. *Phys. Rev. B* **85**(20), 205302 (2012).
36. A. Enyashin, S. Gemming, and G. Seifert: Nanosized allotropes of molybdenum disulfide. *Eur. Phys. J. Spec. Top.* **149**, 103 (2007).
37. H. Terrones, F. Lopez-Urias, and M. Terrones: Novel hetero-layered materials with tunable direct band gaps by sandwiching different metal disulfides and diselenides. *Sci. Rep.* **3**, (2013).
38. J.C. Wildervanck and F. Jellinek: Preparation and crystallinity of molybdenum and tungsten sulfides. *Z. Anorg. Allg. Chem.* **328**(5–6), 309 (1964).
39. P.R. Bonneau, R.F. Jarvis, and R.B. Kaner: Rapid solid-state synthesis of materials from molybdenum-disulfide to refractories. *Nature* **349**(6309), 510 (1991).
40. P.B. James and M.T. Lavik: Crystal structure of $MoSe_2$. *Acta Crystall.* **16**(11), 1183 (1963).
41. A.L. Elías, N. Perea-López, A. Castro-Beltrán, A. Berkdemir, R. Lv, S. Feng, A.D. Long, T. Hayashi, Y.A. Kim, M. Endo, H.R. Gutiérrez, N.R. Pradhan, L. Balicas, T.E. Mallouk, F. López-Urías, H. Terrones, and M. Terrones: Controlled synthesis and transfer of large-area WS2 sheets: From single layer to few layers. *ACS Nano* **7**(6), 5235 (2013).
42. T. Georgiou, R. Jalil, B.D. Belle, L. Britnell, R.V. Gorbachev, S.V. Morozov, Y.J. Kim, A. Gholinia, S.J. Haigh, O. Makarovsky, L. Eaves, L.A. Ponomarenko, A.K. Geim, K.S. Novoselov, and A. Mishchenko: Vertical field-effect transistor based on graphene-WS2 heterostructures for flexible and transparent electronics. *Nat. Nanotechnol.* **8**(2), 100 (2013).
43. S.J. Clark, M.D. Segall, C.J. Pickard, P.J. Hasnip, M.J. Probert, K. Refson, and M.C. Payne: First principles methods using CASTEP. *Z. Kristallogr.* **220**(5–6), 567 (2005).
44. D.M. Ceperley and B.J. Alder: Ground-state of the electron-gas by a stochastic method. *Phys. Rev. Lett.* **45**(7), 566 (1980).
45. J.P. Perdew and A. Zunger: Self-interaction correction to density-functional approximations for many-electron systems. *Phys. Rev. B* **23**(10), 5048 (1981).
46. F. Ortmann, F. Bechstedt, and W.G. Schmidt: Semiempirical van der Waals correction to the density functional description of solids and molecular structures. *Phys. Rev. B* **73**(20), 205101 (2006).
47. J.P. Perdew, J.A. Chevary, S.H. Vosko, K.A. Jackson, M.R. Pederson, D.J. Singh, and C. Fiolhais: Atoms, molecules, solids, and surfaces: Applications of the generalized gradient approximation for the exchange and correlation. *Phys. Rev. B* **46**(11), 6671 (1992).
48. Y. Ding, Y. Wang, J. Ni, L. Shi, S. Shi, and W. Tang: First principles study of structural, vibrational and electronic properties of graphene-like MX2 (M=Mo, Nb, W, Ta; X=S, Se, Te) monolayers. *Physica B* **406**(11), 2254 (2011).
49. S.K. Mahatha, K.D. Patel, and K.S.R. Menon: Electronic structure investigation of MoS_2 and $MoSe_2$ using angle-resolved photoemission spectroscopy and ab initio band structure studies. *J. Phys. Condens. Matter* **24**(47), 475504 (2012).
50. K. Refson, P.R. Tulip, and S.J. Clark: Variational density-functional perturbation theory for dielectrics and lattice dynamics. *Phys. Rev. B* **73**(15), 155114 (2006).

https://doi.org/10.1557/jmr.2013.284 Published online by Cambridge University Press